climate

MDPI

Article

Temporal and Spatial Analyses of Forest Burnt Area in the Middle Volga Region Based on Satellite Imagery and Climatic Factors

Eldar Kurbanov [1,*], Oleg Vorobev [1], Sergei Lezhnin [1], Denis Dergunov [1], Jinliang Wang [2], Jinming Sha [3], Aleksandr Gubaev [1], Ludmila Tarasova [1] and Yibo Wang [1]

[1] Center for Sustainable Forest Management and Remote Sensing, Volga State University of Technology, Yoshkar-Ola 424000, Russia; lejninsa@volgatech.net (S.L.); dergunovdm@volgatech.net (D.D.)
[2] Faculty of Geography, Yunnan Normal University, Chenggong District, Kunming 650500, China; jlwang@ynnu.edu.cn
[3] School of Geographical Science, Fujian Normal University, Fuzhou 350007, China; jmsha@fjnu.edu.cn
* Correspondence: kurbanovea@volgatech.net

Abstract: Wildfires are important natural drivers of forest stands dynamics, strongly affecting their natural regeneration and providing important ecosystem services. This paper presents a comprehensive analysis of spatiotemporal burnt area (BA) patterns in the Middle Volga region of the Russian Federation from 2000 to 2022, using remote sensing time series data and considering the influence of climatic factors on forest fires. To assess the temporal trends, the Mann–Kendall nonparametric statistical test and Theil–Sen's slope estimator were applied using the LandTrendr algorithm on the Google Earth Platform (GEE). The accuracy assessment revealed a high overall accuracy (>84%) and F-score value (>82%) for forest burnt area detection, evaluated against 581 reference test sites. The results indicate that fire occurrences in the region were predominantly irregular, with the highest frequency recorded as 7.3 over the 22-year period. The total forest BA was estimated to be around 280 thousand hectares, accounting for 1.7% of the land surface area or 4.0% of the total forested area in the Middle Volga region. Coniferous forest stands were found to be the most fire-prone ecosystems, contributing to 59.0% of the total BA, while deciduous stands accounted for 25.1%. Insignificant fire occurrences were observed in young forests and shrub lands. On a seasonal scale, temperature was found to have a greater impact on BA compared with precipitation and wind speed.

Keywords: wildfires; forest; climatic factors; monitoring; fire recurrence; remote sensing; machine learning; Landsat; time series; trend analyses

Citation: Kurbanov, E.; Vorobev, O.; Lezhnin, S.; Dergunov, D.; Wang, J.; Sha, J.; Gubaev, A.; Tarasova, L.; Wang, Y. Temporal and Spatial Analyses of Forest Burnt Area in the Middle Volga Region Based on Satellite Imagery and Climatic Factors. *Climate* **2024**, *12*, 45. https://doi.org/10.3390/cli12030045

Academic Editor: Nir Y. Krakauer

Received: 16 January 2024
Revised: 2 March 2024
Accepted: 14 March 2024
Published: 17 March 2024

1. Introduction

In recent decades, the incidence of wildfires has remarkably increased in many parts of the world [1–4]. The frequency of large wildfires in the Russian Federation, for instance, has nearly doubled from 1991 to 2020 compared with the average statistics from 1960 to 1990, leading to a threefold increase in the area of forest burnt [5]. Similar trends have been observed in the USA and Europe, where wildfire disturbances have steadily increased over the past few decades [6–8]. This upward trend is expected to continue in the future due to human-caused climate change, which will have severe consequences for the environment and economy [9–11].

Wildfire is an important natural disturbance factor shaping global forest landscapes [12]. Small-scale and medium-sized wildfires are essential ecosystem processes that burn out ground-level fuels as such leaf litter and fallen branches [13], shape forest structure [14–17], impact species composition [18–20], and facilitate forest regrowth and regeneration at the stand level [21–23]. Controlled burning, also known as prescribed burning, is widely recognised as an effective approach for restoration and forest management [24,25].

On the other hand, large-scale wildfires pose a serious threat, destroying the ecological balance of terrestrial ecosystems [26,27], leading to the loss of bioresources [28–30], and causing extensive damage to both human lives and property [31,32]. These fires have a detrimental impact on the resilience of ecosystems to climate change, resulting in a loss of habitats and biodiversity, and a reduction in forest value and productivity, thereby endangering human life [33]. Additionally, wildfires can lead to a transition from conifer-dominated forests to deciduous-dominated or mixed forests, and in some cases, even non-forest ecosystems [34]. In this context, it is crucial to comprehensively monitor the extent of BA to assess the trends and patterns of forest fire occurrences, identify the underlying drivers, and anticipate future fire occurrences and patterns. Understanding these processes is essential for preserving ecosystems affected by wildfires, estimating post-fire vegetation recovery, and evaluating the effectiveness of different forest management activities [35,36]. Furthermore, it can provide valuable insights for developing targeted climate adaptation strategies and approaches specific to wildfires [37].

Remotely sensed (RS) data offer powerful tools for monitoring post-fire forest patterns, providing quantitative details and insights into post-fire risk mitigation, and facilitating the analysis of historical fire recovery dynamics on multiple spatial and temporal scales [38]. Several studies can be mentioned that have utilised RS to estimate the spatial and temporal dynamics of forest fire patterns on a regional scale over several decades [39–42]. RS and numerous algorithms have been applied to assess three temporal fire effect stages: pre-fire conditions, active fire characteristics, and post-fire ecosystem responses [43–45].

The RS of forest BA mapping is still an active research topic employing advanced techniques that integrate geo-statistics and machine learning methods [38]. Many studies of post-fire vegetation responses are based on the discrimination of spectral bands and vegetation indices (mostly NDVI, dNBR, and EVI) using MODIS, Landsat, SPOT, and Sentinel multitemporal imagery in different regions and forest ecosystems worldwide [46,47]. Another important research direction is the classification of forest succession patterns after wildfires, which can be used to predict the dynamics of future forest cover [48–51]. However, such studies are generally lacking for the territory of the Russian Federation.

Several studies have investigated the dynamics of forest fire behaviour and burnt areas in the different regions of the Russian Federation [13,52–56]. These studies have revealed differences in the sensitivity of forest fire regimes to climate change and fire return interval (FRI) variability across the territory of the Russian Federation. In central Siberia, for example, the FRI in pine ecosystems was estimated to be about 50 years, with low severity and a relatively rapid recovery of litter after a fire [57]. In the southern Siberia ecotone, which features vegetation from both taiga and steppe, the FRI ranges from 25 to 50 years [58,59]. The fire cycles (FC) in Karelia of the North-West Russian Federation increased from 1630 to 1920 (FC = 46 years) and then decreased from 1930 to 2000 (FC = 283 years) [60]. Kukavskaya et al. [16] studied forest disturbances from 1996 to 2015 in Zabaikalsky Krai of the Russian Federation using satellite data and official national fire statistics. Their results showed that about 13% of the total forest area in the region (dominated by Scots pine) experienced multiple burnings during the estimated period. Furthermore, an analysis of Landsat long-term series from 1984 to 2020 revealed that fires burned over 38 million ha of the middle Amur lowland's territory in the Russian Federation, with a high intensity (up to 36) of the FRI [61].

The Middle Volga region, located within the Volga Federal District, is known for its dense forest cover, making it one of the most heavily forested areas in the European part of the Russian Federation (http://www.fedstat.ru, accessed on 12 February 2024). These fires have various environmental impacts, such as loss and fragmentation of natural habitats, disruption of the hydrological cycle, and negative effects on ecosystem functioning and resilience [62,63]. A focused study on BA in the Republic Mari El was conducted as part of the Northern Eurasia Land Cover Dynamics Analysis (NELDA) project (http://www.fsl.orst.edu/nelda/, accessed on 12 February 2024). The study revealed that

approximately one-third (34,228 ha) of the forests that were burned in 2010 were located on pine (*Pinus sylvestris*) plantations established after the 1972 wildfire [11].

Despite a number of the above-mentioned studies, the spatiotemporal distribution of forest BA in the Volga region of the Russian Federation remains understudied. Therefore, the objectives of this study were to estimate the spatial and temporal BA trend pattern from 2000 to 2022 in the Middle Volga region using remote sensing time series, while considering the impact of climatic factors. Specifically, the research aimed to (1) characterise the dynamics of forest fires in the investigated area; (2) estimate trends in the temporal patterns of forest BA; (3) analyse the effect of climatic factors on forest fires and the distribution of burnt area. The trend analysis of the Landsat time series products was performed using the advanced Google Earth Engine (GEE) cloud-based platform, applying JavaScript programming through its API (application programming interface).

2. Materials and Methods

2.1. Study Area

The study area encompasses the Middle Volga region of the Russian Federation, including Nizhegorodskaya and Kirovskaya oblasts, as well as the Republics Mari El, Tatarstan, and Chuvashia (ranging between 54.89556 N and 58.08659 N in latitude and 42.47314 E and 51.5 4785 E in longitude; Figure 1). This region is located in the central part of the East European Plain and is of particular interest due to its extensive natural forests that are reported to be a substantial terrestrial carbon sink [64]. According to the national forest inventory system (https://docs.cntd.ru/document/902268260?marker=6540IN, accessed on 12 February 2024), the northern part of the study area falls within the South Taiga region of the European part of the Russian Federation, while the central and southern parts are classified as coniferous–deciduous (mixed) forests of the European part (Figure 1).

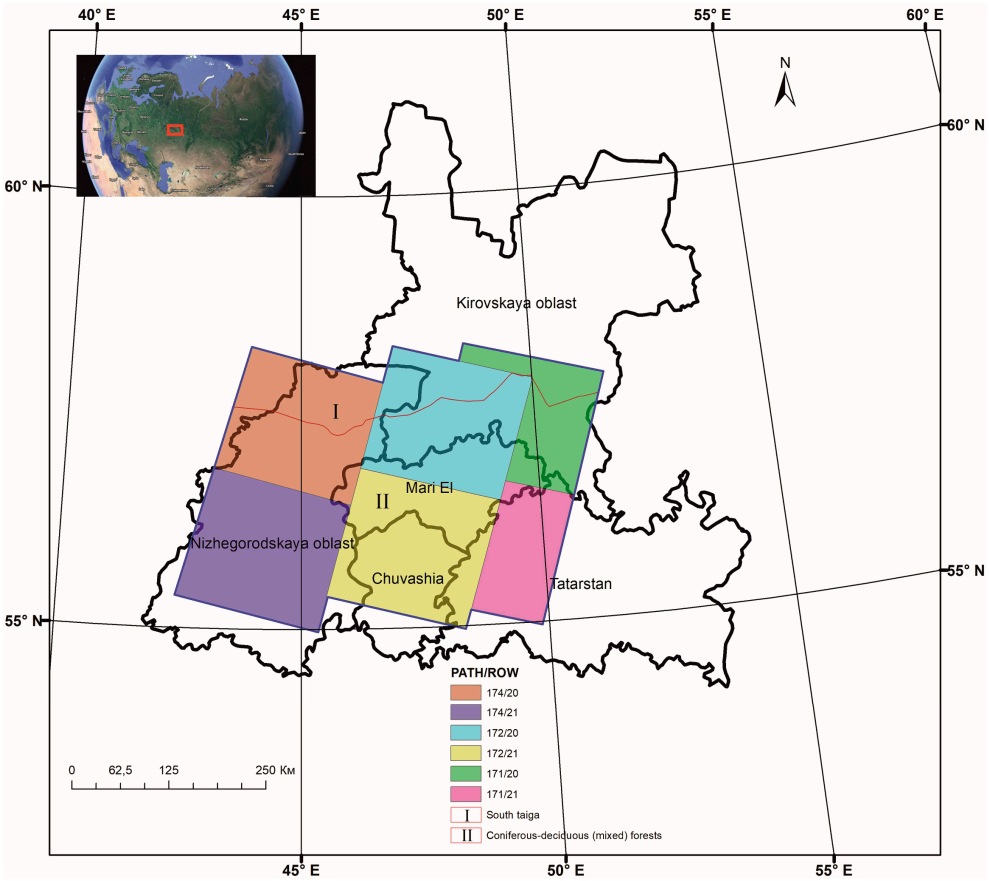

Figure 1. Study area location in the western part of the Russian Federation on the Global map and Landsat scenes.

The Middle Volga region exhibits a diverse relief, ranging from hilly areas to plains, with elevations ranging from 45 to 316 m above sea level. The transition from lower to higher parts is quite gradual. Along the Volga River, there is a central lowland characterised by wide belts of lakes, marshes, and small rivers. The high right bank rises above the valley of the river in the form of a steep ledge with deep ravines [64].

The region's climate is classified as moderate-continental, with relatively stable weather during winter and summer, but significant changes in spring and autumn. The average annual precipitation varies from 450 to 550 mm, with 250–300 mm falling during the vegetation period (spring and summer). Mean annual temperatures vary from +2.2 °C in the north-eastern part of the region to +3.1 °C in the south-western part [65].

The area is dominated by natural coniferous and mixed broadleaved forests, mainly composed of pine (*Pinus sylvestris* L.), birch (*Betula pendula* Roth.), spruce (*Picea abies* Karst.), lime (*Tilia cordata*), and aspen (*Populus tremula* L.). While pine stands dominate the landscape, particularly in the Republic Mari El, the regeneration of birch and aspen species following wildfires is common in the study area. Environmental disturbances such as windstorms, insect outbreaks, and wildfires have become more frequent due to climate change [66]. The significant proportion of broadleaved trees throughout the Middle Volga region can be attributed to the increase in birch trees following forest fires in 1921, 1972, and 2010 [11].

2.2. Data and Method

2.2.1. Remote Sensing

The main approach employed to assess forest BA between 2000 and 2022 involved the processing of Landsat satellite data. A yearly time series of cloud-free surface reflectance medoid data from Landsat (TM, ETM+, and OLI) was extracted for the study area and processed using the JavaScript code editor in the Google Earth Engine (GEE) to generate maps of forest cover and burnt areas. GEE operates in the logic of "Big Data" processing without the need for access to a supercomputer [67]. The platform provides access to a multi-petabyte database of remotely sensed imagery, climate weather data, and geophysical datasets, along with a range of services such as web applications, machine learning tools, and geospatial data visualisation [68]. Previous studies have demonstrated the effectiveness of GEE resources and algorithms in estimating and monitoring forest disturbances, burnt areas, and post-fire vegetation recovery across vast regions [22,45,69]. In particular, the MODIS BA global products [70] available in GEE can be particularly valuable for large-scale analyses and comparison with climate data.

To ensure the accuracy of the analyses, clouds and cloud shadows were automatically detected and removed from Landsat images with the C Function of Mask (CFMASK) algorithm [71]. The selected images were geometrically and atmospherically corrected and converted to surface reflectance using the Landsat Ecosystem Disturbance Adaptive Processing System (LEDAPS) algorithm for TM and ETM+ [72], and the Landsat 8 Surface Reflectance Code (LaSRC) by the USGS for OLI [73]. Since Landsat 8 OLI has a higher 12-bit radiometric resolution compared with the previous ETM+ sensor, the ordinary least squares regression reported in Roy et al. [74] was used to harmonise linear differences between the spectral values of both instruments to normalise the reflectance. To minimise the effect of phenological changes during the spring–summer period, in total, 2393 images covering 6 Landsat scenes (Path 171, 172, and 174; Row 20, 21; Figure 2), were acquired during the forest fire season, which spans from 1 May to 30 September, throughout the entire study period. The time span corresponds to the main dry and wildfire seasons in the Middle Volga region.

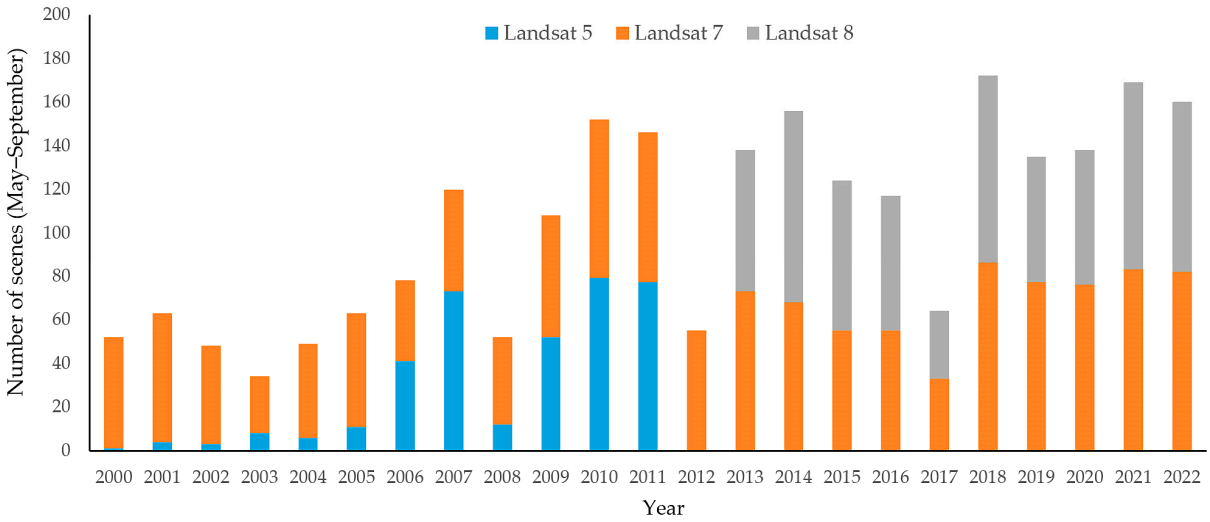

Figure 2. Annual number of Landsat (TM/ETM+/OLI) scene observations over the period May–September 2000–2022.

Supplementary Materials from the Aerial Forest Protection Service of Russia (Avialesookhrana) (https://gfmc.online/emergency/avialesookhrana.html, accessed on 12 February 2024) was utilised to gather additional data on forest fires in the Middle Volga region. The environmental management and ecology agencies of the republics and oblasts in the region also provided valuable information on forest fire occurrences. To distinguish forest fires from other types of disturbances such as logging activities, windfalls, diseases, and pests, MODIS data were also employed. The BA (burnt area) monthly Global 500 m products from MODIS (MCD64A1) were accessed from the FIRMS (Fire Information for Resource Management System) (https://firms.modaps.eosdis.nasa.gov, accessed on 12 February 2024). These data, along with the coordinates and dates of forest fire events between 2000 and 2022, were extracted for the study area. In order to separate the area affected by forest fires from non-fire events, the extracted forest fire data and MODIS data were overlaid and compared with potential disturbance points. This process assisted in accurately identifying the areas impacted by forest fires. Figure 3 illustrates the overall methodology and workflow used in this research.

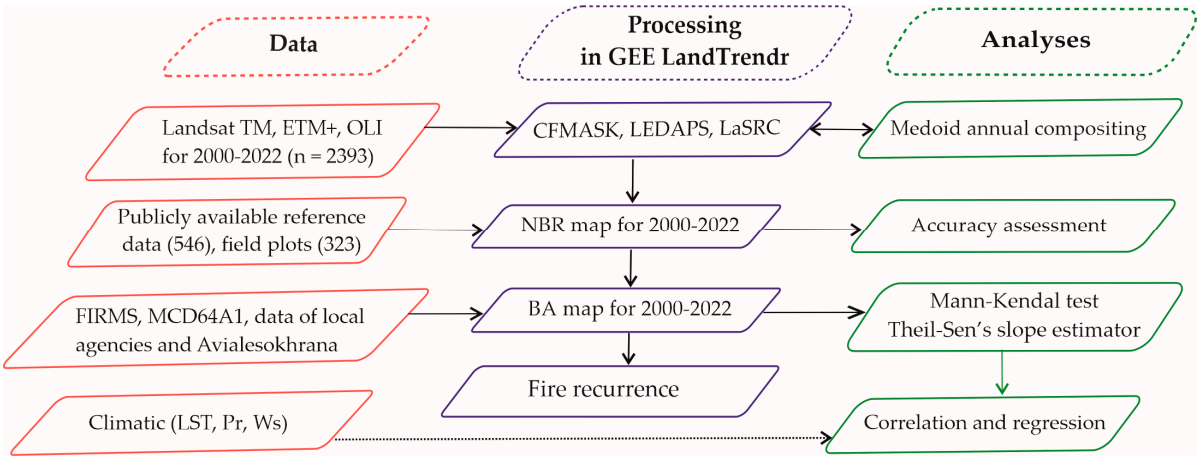

Figure 3. Flow chart of the research.

2.2.2. Temperature, Precipitation, and Wind Speed

The climate data for the Middle Volga region from 2000 to 2022 (May to September) were acquired from a number of gridded datasets (Table 1). We used the MOD11A1

and MOD11A2 archive datasets for the estimation of the average monthly land surface temperature (LST) values in Celsius (°C) at a 1 km spatial resolution and with an 8-day composite (https://ladsweb.modaps.eosdis.nasa.gov/archive/allData, accessed on 12 February 2024). We also used the Global Precipitation Measurement (GPM) IMERG (Integrated Multi-satellitE Retrievals for GPM) Final Precipitation L3 Half Hourly 0.1° × 0.1° V06 (GPM_3IMERGHH) product to determine the gridded monthly average precipitation (Pr, mm/month) values in the studied region (https://giovanni.gsfc.nasa.gov/giovanni/, accessed on 12 February 2024). To determine the monthly average surface wind speed (Ws, m/s) in the research area, we obtained data from the MERRA-2 collection (Modern-Era Retrospective Analysis for Research and Applications version 2) produced by NASA Global Modelling and Assimilation Office (GMAO) (https://disc.gsfc.nasa.gov/datasets/M2TMNXFLX_5.12.4/summary, accessed on 12 February 2024).

Table 1. Data employed for burnt area estimation and climatic factor monitoring in the Middle Volga region from May to September 2000–2022.

No	Purpose	Data, Product ID	Scale	Source
1	BA Mapping	Landsat time series	30 m	https://earthengine.google.com/ (accessed on 12 February 2024)
2		MODIS MCD64A1	500 m	
3		FIRMS		https://firms.modaps.eosdis.nasa.gov (accessed on 12 February 2024)
4	Land surface temperature, Maximum temperature	8-day composite MOD11A1 MOD11A2	1 km	https://ladsweb.modaps.eosdis.nasa.gov/archive/allData (accessed on 12 February 2024)
5	Precipitation	GPM_3IMERGHH	0.1° × 0.1°	https://giovanni.gsfc.nasa.gov/giovanni/ (accessed on 12 February 2024)
6	Wind speed	MERRA-2 GMAO	0.5° × 0.625°	https://disc.gsfc.nasa.gov/datasets/M2TMNXFLX_5.12.4/summary (accessed on 12 February 2024)
7	Validation, accuracy assessment	Google Earth Yandex Maps	10–30 m	www.googleearth.com (accessed on 12 February 2024) https://yandex.ru/maps (accessed on 12 February 2024)
8		Field plots of Volgatech	90 × 90 m	

We also created a regular grid with a cell size of 1 × 1 km covering the BA in the Middle Volga region for each of the estimated years, 2000–2022. For each cell, we determined the values of the climatic parameters (LST, precipitation, and wind speed) at the centre of the cell and estimated the area of burnt forest. Correlation analyses and multivariate linear regression were then applied for each cell's centre to assess the degree of influence of BA and the climatic parameters. We considered all possible temporal aggregations of the climate variables throughout the study period. The correlation and regression coefficients calculated for each grid cell were analysed at both monthly and annual spatial scales. To evaluate the performance of the best-fit regression model, we assessed the estimated BA against the climatic factors (either jointly or separately) using metrics such as root mean square error (RMSE), mean square error (MSE), and coefficient of determination (R^2).

2.2.3. LandTrendr Algorithm

In order to trace the dynamics of burnt forest areas, the prepared stacks of Landsat images were analysed using the LandTrendr (LT) algorithm in the GEE platform [75]. The LT algorithm, implemented in JavaScript, processes the time series of individual values for each Landsat image pixel in each year. It employs a temporal segmentation algorithm and a fitting approach to ensure a consistent time series and minimise sensor influences. For our analyses, we processed the stack of Landsat images using a medoid selection process [76], which is a multi-dimensional analogue of the median. We used the buildSRcollection

code to select the medoid technique from Landsat TM/ETM+/OLI data and compared the spectral values to the median spectral values of each pixel across all visible and infrared bands in all acquired images. LT then selected the pixel with the minimum sum of squared differences between observations and median spectral values, using Euclidean distance. This reduced the data volume and mitigated atmospheric impact [77]. As a result, we obtained an aggregated stack of Landsat images for a 22-year time series, with interpolated spectral values and reduced year-to-year noise. To examine the relationship between forest fires and other factors (LST, Pt, and Ws), we converted the selected pixels of the time series into a normalised burn ratio (NBR), which is the most widely used index for mapping burned areas [78]. Additionally, we applied a spatial filter with a minimum burned area unit of 0.5 ha and excluded isolated and border pixels using neighbourhood filters to improve the spatial consistency of burnt area mapping.

When applying LT-GEE with the NBR, we employed the following parameter values: "max-segments = 3", "*p*-value = 0.05", "Recovery threshold = 0.25", and "Vertex Count Overshoot = 3" [75]. To generate the BA mosaic, we filtered Landsat imagery dates to include only the years 2000–2022 and the season from May to September. BAs were identified if at least 3 segments were detected during the entire study period and there was a noticeable decrease in the NBR index value within a one-year period.

To estimate the monotonic trend behaviour ($p < 0.05$) of the factors LST, Pr, and Ws based on the Landsat time series, we employed the GEE kendallsCorrelation algorithm to conduct the Mann–Kendall (MK) nonparametric statistical test (TAU-b rank correlation). This test assumes that observations within a time series are independent [79,80]. A positive value from this test shows an upward trend, while a negative value indicates a downward trend. The rate of change and magnitude of the trends in estimated factors were evaluated in GEE using Theil–Sen's slope estimator, a non-parametric technique for assessing the median slope [81,82]. These tests have been recommended by the World Meteorological Organization for climate studies and have proven successful in trend analyses of environmental data [83–85].

2.2.4. Reference Data and Statistical Validation

In order to validate the forest BA mapping and trend analysis, we randomly identified 546 forest BA samples from 2000 to 2022 on the basis of high-resolution satellite imagery from publicly available Google Earth and Yandex Maps platforms for the investigated territory using the visual interpretation method [86]. In addition, field campaigns were carried out by the Volgatech team during the summer period (June–August) of 2011, 2012, 2014, 2017, 2019, 2020, and 2022 in the BA of the Middle Volga region. Sample plots, measuring at least 90 by 90 m, were chosen to represent a range of stand age groups, tree species, and typical structures found in the region. Measurements such as diameter at breast height (DBH) at 1.3 m, tree height, char height, and crown length were collected for each tree using a laser clinometer and metre tape to assess tree mortality (standing or fallen). The sample plots, totalling 323, were randomly distributed primarily in conifer and broadleaved mixed stands within the burnt areas of the investigated territory. Furthermore, for the estimation of woody detritus on the sample plots, stumps and logs with a diameter exceeding 10 cm and a length of more than 1 m in length were measured [13]. These sample plots were representative of the overall characteristics of the investigated area, including forest type, altitude, and climate.

The gathered set of sample plots served as input data for the confusion matrices and served to estimate the accuracy of burnt area detection derived from the Landsat images. Only two classes (burnt area and non-burnt area) were considered in the confusion matrix. The accuracy assessment of the BA maps was based on comparing the proportions for each pixel detected as burnt or unburnt in the Landsat images with the prepared reference data. Four accuracy metrics derived from confusion matrices were calculated to validate the BA detection: the user's accuracy (UA), the commission error (CE), the producer's accuracy

(PA), and the omission error (OE) [87]. Additionally, we computed the overall accuracy (OA) and F-score, which provide an estimate of the test's accuracy.

3. Results

3.1. Accuracy Assessment

The Landsat time series imagery from 2000 to 2022 was utilised to analyse the spatial distribution of burnt areas (BAs) in the Middle Volga region using the NBR LandTrendr data. Figure 4 shows the spatial distribution of BAs in the region, while Table S1 (Supplementary Materials) presents the error matrix derived from the reference set of samples. To validate the statistical accuracy of BA mapping, a visual interpretation of 869 test sites (equivalent to 7901 pixels) was conducted to evaluate the user's accuracy (UA), producer's accuracy (PA), overall accuracy, and F-score between the Landsat time series and the reference set of samples. The BA mapping demonstrated high accuracy, with an overall accuracy of 84.5% over the 22-year period (Table S1 in the Supplementary Materials). Both the user's and producer's accuracies exceeded 80%, while the F-score value reached 82%. These results indicate that the LandTrendr mapping analyses were consistently accurate and reliable, making the final BA map suitable for subsequent analysis with climatic factors.

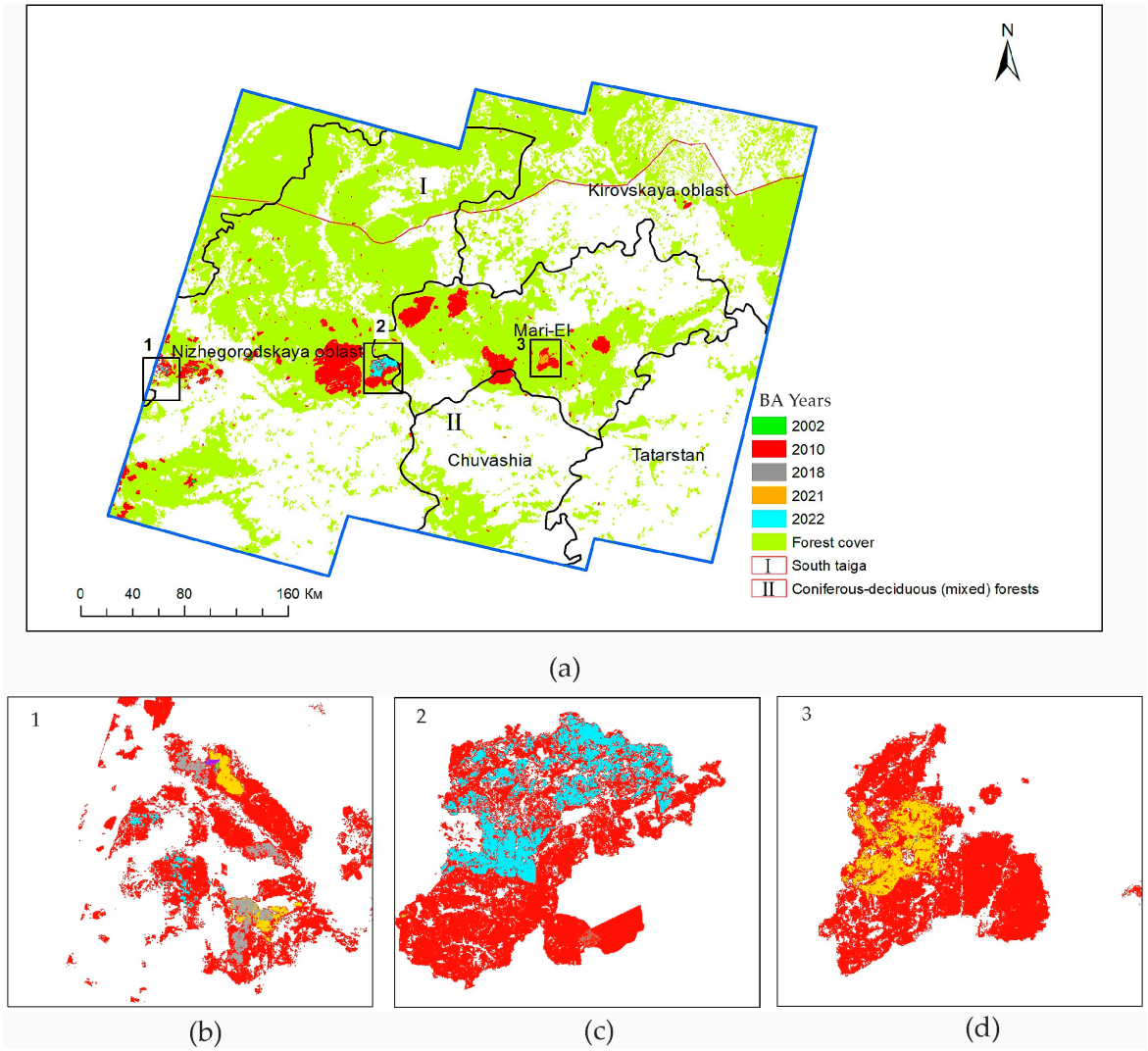

Figure 4. Spatial distribution of cumulative forest BA from 2000 to 2022: (**a**) overall Middle Volga region, (**b**) burnt three times in Nizhegorodskaya oblast, (**c**) burnt two times in Nizhegorodskaya oblast and Mari El, (**d**) and burnt two times in the Republic Mari El. The pixel size is exaggerated for visualisation purposes.

3.2. Spatial and Temporal Distribution of BA in the Middle Volga

We observed that occurrence of BA is widespread throughout the study region, with burnt areas predominantly spatially located in the western and central parts of the Middle Volga forests. Over the course of the past 22 years, the total forest BA covered approximately 280 thousand ha, which accounts for 1.7% of the land surface area or 4.0% of the total forested area (6881 mln. ha) in the studied territory of the Middle Volga region. We observed significant inter-annual variations among the 318 identified BAs across the investigated forest area, ranging from 0.075 to 244 thousand ha (Figure 4a). As can be seen from Figure 4, there are BAs in all oblasts and republics of the region, while most of them are concentrated in the forest cover of the Republic Mari El and Nizhegorodskaya oblast. The smallest identified wildfire in the Middle Volga region affected a forest area of 0.5 ha, while the largest identified BA covered 86.6 thousand ha in the Nizhegorodskaya oblast (Figure 5b).

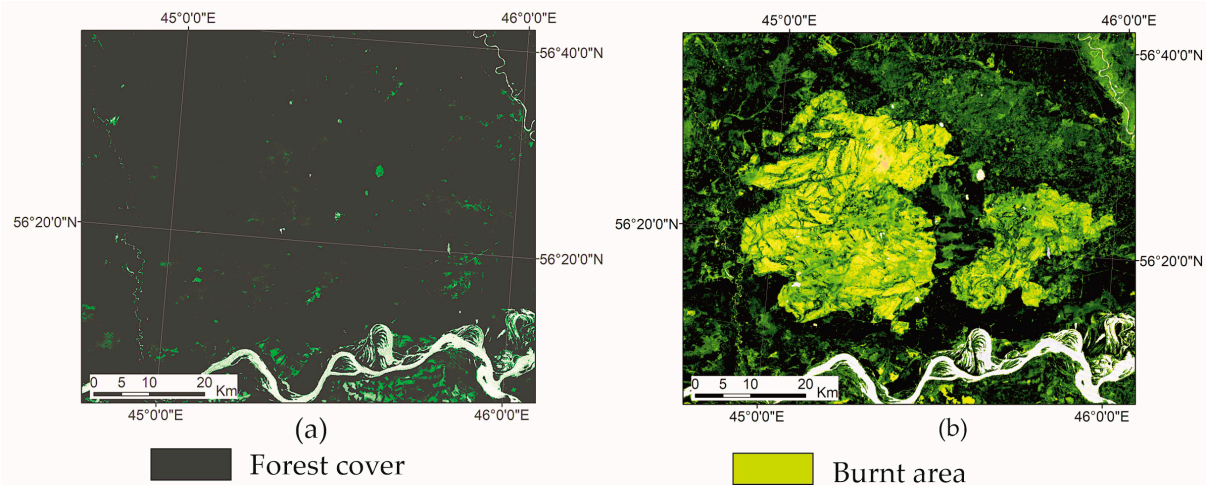

Figure 5. NDVI of the forest cover in Nizhegorodskaya oblast on the Landsat 5 TM images: (**a**) September 2009; (**b**) October 2010 (after the wildfire).

The largest forest BA observed on the investigated territory was 244.2 thousand ha, which occurred after the disastrous wildfires of 2010 (Figure 6a). This event had a significant impact on the distribution of BAs during the study period. To analyse the spatial and temporal distribution of BAs during years with relatively few wildfires, some calculations and figures in the study were made without considering this anomalous year (Figure 6b–d).

The annual average BA in the region was 12.2 thousand ha. The overall polynomial trend (R^2 = 0.65) indicates that the averaged BA after the 2010 wildfires has been increasing by 1.970 thousand ha/year (Figure 6b). The second and third largest forest BAs were detected in 2002 and 2021–2022, with areas of about 5.1 thousand ha and 18.4 thousand ha, respectively. Both of these peaks in BA followed a decade-long period of relatively infrequent wildfires. This is particularly evident in the case of the 2021 forest fires, where only 5.325 thousand ha (0.08% of the forested area) burned between 2010 and 2020. The smallest BA of 76 ha was observed in this region in 2008.

The BA data analysis reveals that the majority of forest fires in the Middle Volga region occurred during the summer dry season, specifically between June and August. During this period, the average monthly precipitation was less than 50 mm, the average wind speed was 5 m/s, and the average temperature was 26.4 °C. The largest forest BA, averaging 21.232 thousand ha, was observed in July (Figure 6c,d); it was 1.5 thousand ha when not considering the abnormal wildfires in 2010. Throughout the vegetation season, the average BA was 0.256 thousand ha in May, 2.575 thousand ha in June, and 0.656 thousand ha in August.

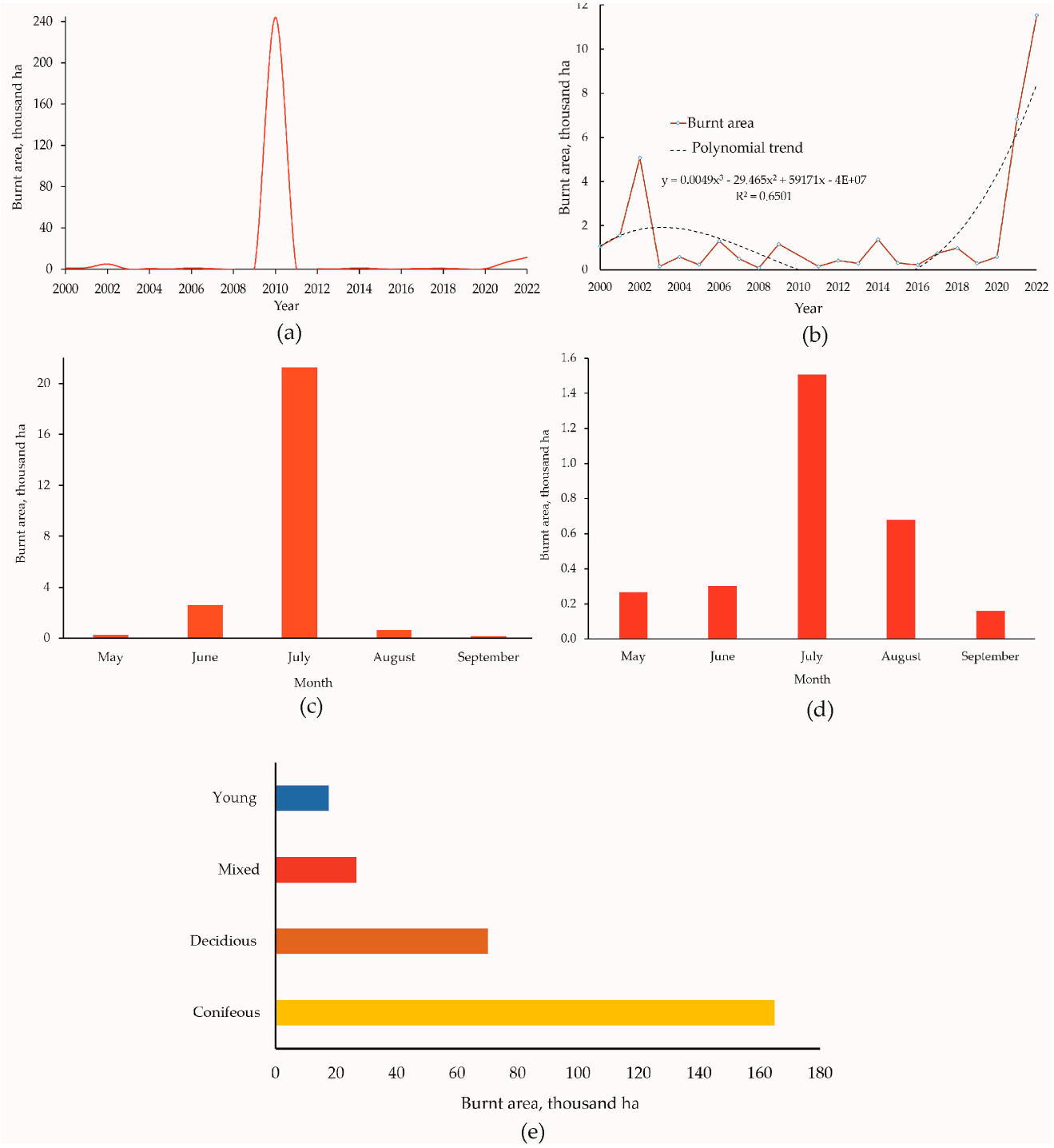

Figure 6. Dynamics of forest burnt area in the Middle Volga region from 2000 to 2022, (**a**) including the severe wildfires of 2010, and (**b**) those excluding the data of 2010 wildfires. (**c**) The mean monthly forest BA with data on 2010 wildfires, (**d**) and the mean monthly BA without data on 2010 wildfires. (**e**) Cumulative BA according to the forest classes.

The analysis also revealed that most wildfires occurred in coniferous and deciduous forest stands, while young forests and shrub-dominated lands were less susceptible to fire hazards. Coniferous forest stands, primarily consisting of middle-aged and mature pine and spruce species, accounted for 59.0% (164.9 thousand ha) of the total BA (Figure 5e). Deciduous stands, mainly composed of middle-aged and mature birch and poplar species, accounted for 25.1% (70.2 thousand ha) of the BA. Mixed forest stands accounted for 9.6%

(approximately 26.8 thousand ha) of the BA, while young forests, including plantations and shrublands, accounted for 6.3% (17.7 thousand ha) (Figure 6e).

3.3. Fire Recurrence in the Middle Volga Region

The recurrence of wildfires in certain forested areas of the Middle Volga region has led to significant disturbances. Between 2000 and 2022, approximately 279.524 thousand ha (4%) of forests in the analysed region experienced at least one fire. The other 96% of the forested area remain unburnt, but there were significant variations across the study area. The Republic Mari El and Nizhegorodskaya oblast were particularly affected, with fires occurring in 7.8% and 4.9% of their forested areas, respectively. The Chuvashia Republic exhibited high forest fragmentation, resulting in a cumulative burnt area covering only 3.2% of the forested area with low connectivity. Additionally, this region experienced minimal fire recurrence, with most of the burnt area having no repeated fires over the 22-year period.

The analysis of forest fire frequency from 2000 to 2022 (see Figure 4) reveals that fire occurrences in the region are predominantly irregular, with the highest wildfire frequency recorded as 7.3 over the 22-year period. The maximum fire recurrence (three times) during the study period was observed in a small area of 363 hectares, accounting for 0.1% of the overall burnt area, in the forests of Nizhegorodskaya oblast (see Figure 4b). Only 8593 hectares (3%) of the burnt area experienced two fires within the same location over the 22-year period (see Figure 4c,d), with these wildfires primarily occurring in the Mari El and Nizhegorodskaya oblast. The analysis of burnt area occurrence within the research area boundaries indicates that the highest fire activity mainly affected the territory of coniferous–deciduous (mixed) forests (99.5%) in the European part of the Russian Federation. The South Taiga region experienced relatively fewer disturbances, with wildfires mainly occurring in 2010 on a small area (0.5%) in the Kirov region of the Middle Volga region. Most of the recurrent wildfires were observed in coniferous and deciduous forest areas, while mixed stands showed fewer instances of repeated burnt areas.

3.4. Effect of Climatic Factors on BA in the Middle Volga Region

3.4.1. Spatiotemporal Trend Analyses

Based on the Mann–Kendall τ (tau) correlation coefficient and Theil–Sen's slope (TSS) analysis, the trend of the climatic parameters on a pixel scale was analysed for the forest area during the vegetation season in the Middle Volga region over the period 2000–2022 (Table 2). Figure 7 shows the monotonic trends of tau and TSS in the Landsat time series for the mean LST, Pr and Ws, highlighting areas with an increasing trend (in red) and a decreasing trend (in blue).

Table 2. Trends of climatic factors in the Middle Volga region over the period 2000–2022 at a 95% confidence level.

Parameter	Trend	Tau (τ)	Theil–Sen's Slope	*p*-Value
Temperature	Increasing	0.05	0.014	0.02
Precipitation	Decreasing	−0.29	−0.27	0.05
Wind	Increasing	0.03	0.09	0.03

The values presented in Table 2 represent the average correlation of each pixel in the time series. The eastern part of the investigated region, which experienced infrequent wildfire occurrences, shows the largest decreasing trend with a slope of −0.27 in Pr (Figure 7b, Table 2). Conversely, the central and western parts of the region (Mari El and Nizhny Novgorod), corresponding to the main forest BA, show increasing trends in LST. This indicates a rise in temperature in these areas during the vegetation season. The impact of precipitation (Pr) on BA is generally positive throughout the investigated territory, as shown in Figure 7b. Increased precipitation, particularly in the eastern part of Mari El and the western part of Tatarstan, leads to a reduction in forest fire occurrences. Furthermore,

the magnitude of wind speed (Ws) is generally high in the eastern and central forested parts of the region, while it is low in the west (Figure 7c). Overall, the analysis suggests that the contribution of LST to BA in the Middle Volga region during the vegetation season is more significant compared with that of Pr and Ws.

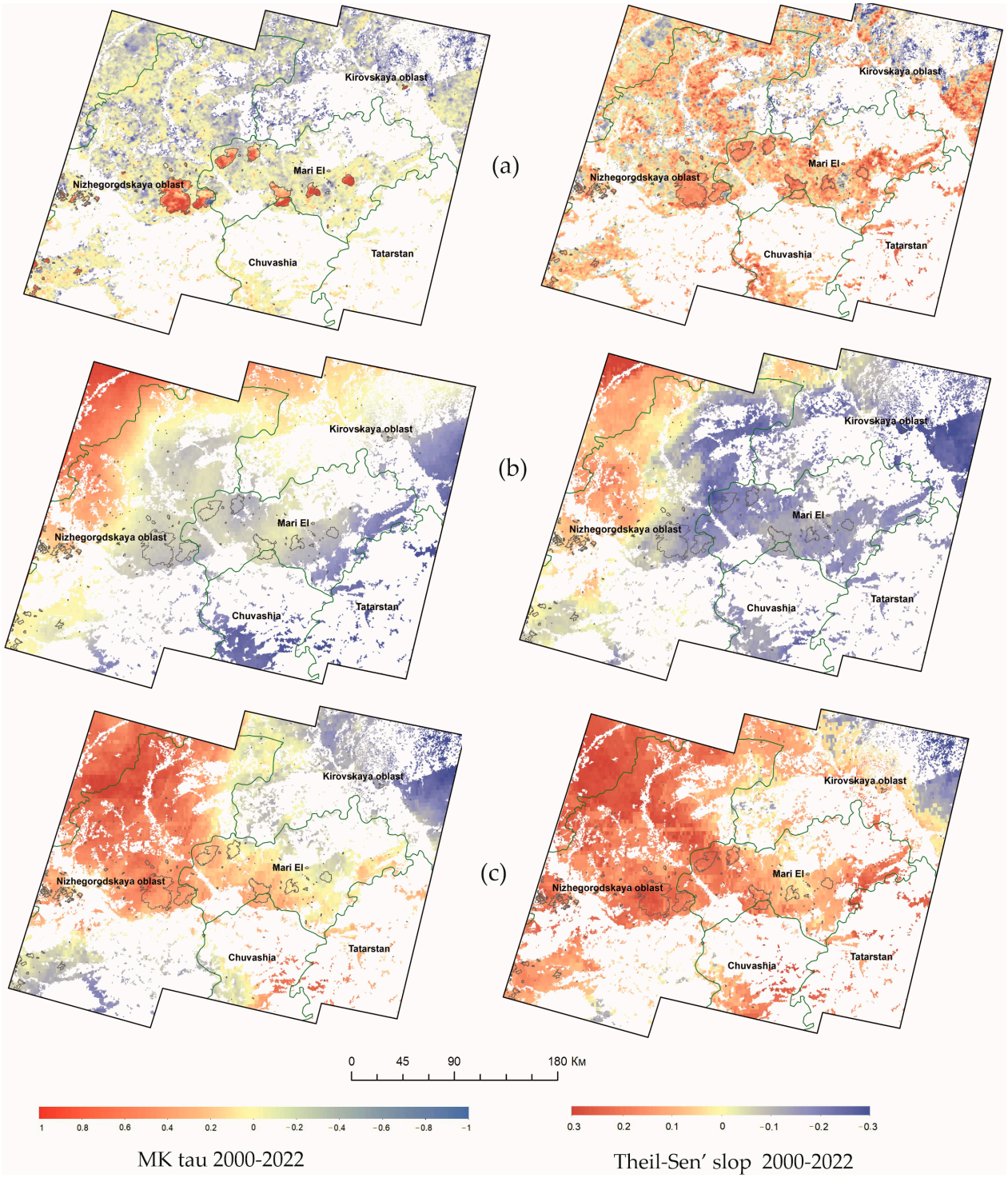

Figure 7. Mann–Kendall tau (strength) and Theil–Sen's slope (magnitude) trend analysis for climatic factors in the Middle Volga region with BA from 2000 to 2022: (**a**) land surface temperature; (**b**) precipitation; (**c**) wind speed. The highest level of rank correlation for pixel trends using the both methods falls near 1 and 0.3 (deep red for positive trends) or −1 and −0.3 (deep blue for negative trends).

3.4.2. Regression Analyses of Climate Data and BA

The correlation analyses results (Figure 8) indicated that climatic factors played a relatively important role in the BA trend during the investigated period. Among the climatic variables, temperature (LST) shows a stronger impact on BA compared with precipitation. To further understand the relationship between climate and BA, a multivariable regression model was developed, taking into account the monthly mean values of LST, wind speed (Ws), and precipitation (Pr) averaged from May to September over the entire study period (2000–2022). The best equation with a higher fit of combined climatic factors considered (p-value < 0.05) was the one using the monthly mean of LST, Wt and Pr averaged over the estimated period (May to September):

$$BA = -16.4 + 0.32 * LST - 0.01 * Pr + 2.2 * Ws,\ R^2 = 0.36$$

The model, with a fitted R^2 statistic of 36%, indicates that the combined climatic factors of LST, Ws, and Pr significantly influence the distribution of BA (Figure 8). The spatial correlation between BA and Ws was particularly strong in the western and central parts of the region during May and July (R^2 = 0.48). In September, there was a positive correlation between LST and BA (R^2 = 0.58), while the effects of Pr and Ws were weak (<0.28) and insignificant. Meanwhile, in July, both Pr and Ws were considered important variables. The main driving climatic factors for BA were different during the vegetation season, and therefore it is challenging to determine a single one as the main contributor to the forest fires in the region.

Climatic Factor	Month				
	May	June	July	August	September
BA—Precipitation	0.27	−0.30	**−0.68 ***	−0.25	0.25
BA—Wind speed	**0.48 ***	0.06	0.46	0.36	0.28
BA—Temperature	0.43 *	**0.60 ***	0.31	**0.59 ***	**0.58 ***

Pearson Product–Moment Correlation

−1.0 1.0

Figure 8. Correlation coefficients between BA and climatic factors during 2000–2022 spring-autumn seasons; * indicates that the values passed the significance test (p < 0.05).

4. Discussion

This study provided a trend analysis of the spatial and temporal patterns of forest burnt areas in the Middle Volga region of the Russian Federation from 2000 to 2022 using Landsat time series images. We took advantage of the LandTrendr algorithm in the GEE cloud computing environment to estimate the influence of the degree of climatic factors (LST, Pt, and Ws) on the BA distribution and forest fire recurrence on a large spatiotemporal scale. Our results confirmed the high potential of using the GEE platform to consistently and cost-effectively estimate BA on large forest lands, since the platform provides easy access to a large number of satellite data resources. The GEE also offers many useful ready-made products, machine learning algorithms, and the possibility of simple programming in a JavaScript environment [67,68].

To evaluate the accuracy of the produced maps, a confusion matrix and various indices were employed, using reference data from publicly available platforms like Google Earth and Yandex Maps. Ground sample plots were also randomly distributed throughout the studied burnt areas. The inclusion of field survey data was crucial as it helped identify small burnt areas that were not recognised from Landsat imagery alone. The overall accuracy was higher than 84%, and the F-score value was 82%, which shows that the results of the proposed algorithm were reliable for detecting burnt and unburnt forest areas in the investigated region.

During the study period of 2000–2022, our analysis revealed that approximately 280 thousand ha (4.0% of the total forested area) in the Middle Volga region was affected by wildfires. Across this area, a significant proportion consisted of burnt coniferous stands, accounting for 59% of the total burnt area. The distribution of burnt areas varied across different republics and oblasts within the Middle Volga region, with the Republic of Mari El and Nizhegorodskaya oblast experiencing the highest levels of fire activity.

The occurrence of wildfires in the forested areas was predominantly sporadic, with the years 2002, 2010, and 2021 exhibiting the highest frequency of fire events (Figure 6a,b). The South Taiga region, on the other hand, experienced relatively lower levels of wildfire disturbance. Notably, around 3% of the burnt areas was affected by wildfires twice during the 22-year period, primarily in coniferous plantation forests, particularly those dominated by Scots pine. These dense young stands are particularly vulnerable to fire, as the lower branches act as ladder fuels, facilitating the spread of fire from the ground to the tree crowns [11]. While pine species are favoured for their natural ability to release seeds after a wildfire and their suitability for industrial wood production, the regeneration of coniferous stands in the Middle Volga region increases the risk of wildfires, posing a direct threat to local communities and property. It is important to consider these factors in post-fire management plans and take necessary measures to mitigate the danger of wildfires in the region.

The significance of climatic factors in estimating burnt areas (BA) using satellite imagery has been recognised in various regions worldwide [88,89]. Our study findings indicate that Theil–Sen's slope estimate and the Mann–Kendall tau test, applied in the long-term Landsat trend analysis of climatic factors, serve as suitable indicators for predicting the occurrence and spread of wildfires across the vast territory of the Middle Volga region. Through LandTrendr and regression analyses, we observed a significant influence of estimated climatic factors on wildfires (burnt areas) in the region, with a confidence level of 95%. Among the climatic factors, LST emerged as the most important, exhibiting a stronger correlation with forest BA compared with the other two factors. During the spring–autumn seasons, the central and western parts of the region (Republic Mari El and Nizhegorodskaya oblast), characterised by coniferous and deciduous forest stands, experienced trends of increasing LST.

The precipitation (Pr) factor is also important, following LST, in evaluating the spatiotemporal distribution of BA in terms of the correlation coefficient and trend analyses during the burning seasons (see Figures 7 and 8). Since the 21st century, there has been a decreasing trend for precipitation in the majority of BA in the Middle Volga region. The central and southwestern forest areas are more prone to drought compared with the northwestern parts of the region. Therefore, if these climatic trends continue in the future, high temperatures and low rainfall during the spring–summer season can easily lead to wildfires. The wind speed (Ws) factor, which shows an increasing spatiotemporal trend throughout the forest area, is also positively correlated with BA. The significant positive correlations between Ws and BA mainly occur in May and July. Strong winds and higher LST in spring and summer also reduce the moisture content of the forest floor combustibles, thereby increasing the probability and duration of fire outbreaks. Ultimately, these three climatic factors (LST, Pr, and Ws) are crucial in understanding the impacts of climate change on the increased fire activity observed over the past two decades.

Although important results were obtained in this study, further research is needed to improve and broaden the scope of the analyses carried out. Besides climatic factors, forest BA can also be influenced by various other driving factors, including topography, forest stand structure, undergrowth composition, soil moisture, forest litter, and socio-economic data specific to each satellite image. However, due to the lack of reliable ground truth data in remote forest areas of the Middle Volga region and the limited temporal, spectral, and spatial resolution capabilities of Landsat imagery [90], some smaller BA values were not detected in the estimated time series data. One potential solution to address these limitations could be the combination of Landsat and Sentinel imagery [91–93], the utilisation

of more sensitive spectral indices, and supplementation with field survey data. Future research in the field of BA should also aim to improve attribution algorithms and explore alternative climate change scenarios for improved forest management policies, land use practices, and resilience strategies that explicitly consider the prevention or adaptation of forest ecosystems to the changing environment.

We suggest that our methodology can be applied to map forest BA and estimate trends in climatic factors in other coniferous–deciduous forest regions of the Russian Federation, as it has demonstrated high detection accuracy in the diverse and extensive landscapes of the Middle Volga region. The generated maps, regression models, and trend analysis of climatic factors, at a spatial resolution relevant to forest management and monitoring, can be valuable tools for local authorities and decision makers in strategic planning to prevent or mitigate the risk of wildfires. Priority should be given to regions prone to widespread forest fires, such as the Republic Mari El and Nizhegorodskaya oblast, when implementing fire protection activities.

5. Conclusions

This research demonstrates the practicality of using the LandTrendr algorithm in the Google Earth Engine platform to analyse long-term trends in pre-processed NBR Landsat time series data. The study focuses on detecting and mapping the temporal dynamics of forest burnt areas in the Middle Volga region of the Russian Federation. By analysing the interaction between forest burnt areas and climatic factors, the study provides valuable insights into the characteristics and patterns of burnt areas from 2000 to 2022 on both regional and seasonal scales. This research achieves a high overall accuracy (>84.0%) using deep learning algorithms, indicating our methodology's cost-effectiveness and success in analysing large-scale spatiotemporal remote sensing data of wildfire-affected forests. This study reveals an increasing trend for forest BA annually across the Middle Volga region, with the highest concentration found in the central and western parts, particularly in coniferous ecosystems (59%). This study also identifies three climatic factors, namely LST (land surface temperature), Ws (wind speed), and Pr (precipitation), as indicators for projecting the occurrence and dynamics of wildfires during the late spring–summer period. These findings have significant implications for environmental studies, including carbon forecasting in forest ecosystems, vegetation regeneration, and climate-smart forestry. Furthermore, this research can inform management decisions by providing cost-effective strategies for preventing forest fires under changing climatic conditions.

Supplementary Materials: The Supplementary Materials can be downloaded at https://www.mdpi.com/article/10.3390/cli12030045/s1: Table S1. Confusion matrix for accuracy assessment of BA detection.

Author Contributions: Conceptualisation, E.K., O.V., J.S. and J.W.; methodology, E.K., O.V., J.S. and J.W.; software, S.L., D.D., A.G. and Y.W.; validation, E.K., O.V., S.L., D.D. and L.T.; formal analysis, E.K., O.V., J.W. and S.L; investigation, O.V., S.L., D.D., A.G., L.T. and Y.W.; resources, S.L., A.G., L.T., D.D. and Y.W.; data curation, S.L., D.D., A.G. and L.T.; writing—original draft preparation, E.K. and O.V.; writing—review and editing, E.K., J.S., O.V. and J.W.; visualisation, D.D., A.G., S.L. and Y.W.; supervision, E.K.; project administration, E.K., J.S. and J.W.; funding acquisition, E.K. All authors have read and agreed to the published version of the manuscript.

Funding: The reported study was funded in the framework of the Russian Science Foundation, grant No. 22-16-00094, https://rscf.ru/project/22-16-00094/ (accessed on 5 March 2024).

Institutional Review Board Statement: Not applicable.

Informed Consent Statement: Not applicable.

Data Availability Statement: The data presented in this study are available in the article. More information is available on request from the corresponding authors.

Acknowledgments: The authors are grateful to the anonymous reviewers for their valuable feedback and guidance in improving the initial version of this manuscript in multiple ways.

Conflicts of Interest: The authors declare no conflicts of interest. The funders had no role in the design of the study; in the collection, analyses, or interpretation of data; in the writing of the manuscript; or in the decision to publish the results.

References

1. Turco, M.; Abatzoglou, J.T.; Herrera, S.; Cvijanovic, I. Anthropogenic climate change impacts exacerbate summer forest fires in California. *Proc. Natl. Acad. Sci. USA* **2023**, *120*, e2213815120. [CrossRef]
2. Li, Y.; Wu, Z.; Xu, X.; Tong, X.; Liu, J. Forest disturbances and the attribution derived from yearly Landsat time series over 1990–2020 in the Hengduan Mountains Region of Southwest China. *For. Ecosyst.* **2021**, *8*, 73. [CrossRef]
3. Špulák, P. Wildland fires in the Czech Republic—Review of Data Spanning 20 Years. *ISPRS Int. J. Geo-Inf.* **2022**, *11*, 289. [CrossRef]
4. Molina-Terren, D.M.; Xanthopoulos, G.; Diakakis, M.; Ribeiro, L.; Caballero, D.; Delogu, G.M.; Viegas, D.X.; Silva, C.A.; Cardil, A. Analysis of forest fire fatalities in Southern Europe: Spain, Portugal, Greece and Sardinia (Italy). *Int. J. Wildland Fire* **2019**, *28*, 85–98. [CrossRef]
5. Federal State Statistic Service. Statistika Okruzhayushchej Prirodnoj Sredy i Prirodopol'zovaniya. FSSS. Available online: https://rosstat.gov.ru (accessed on 4 December 2023). (In Russian)
6. Cohen, W.B.; Yang, Z.; Stehman, S.V.; Schroeder, T.A.; Bell, D.M.; Masek, J.G.; Huang, C.; Meigs, G.W. Forest disturbance across the conterminous United States from 1985–2012: The emerging dominance of forest decline. *For. Ecol. Manag.* **2016**, *360*, 242–252. [CrossRef]
7. Iglesias, V.; Balch, J.K.; Travis, W.R. U.S. fires became larger, more frequent, and more widespread in the 2000s. *Sci. Adv.* **2022**, *8*, eabc0020. [CrossRef] [PubMed]
8. Parente, J.; Tonini, M.; Stamou, Z.; Koutsias, N.; Pereira, M. Quantitative assessment of the relationship between Land Use/Land Cover Changes and wildfires in Southern Europe. *Fire* **2023**, *6*, 198. [CrossRef]
9. Kalogiannidis, S.; Chatzitheodoridis, F.; Kalfas, D.; Patitsa, C.; Papagrigoriou, A. Socio-psychological, economic and environmental effects of forest fires. *Fire* **2023**, *6*, 280. [CrossRef]
10. Lindner, M.; Maroschek, M.; Netherer, S.; Kremer, A.; Barbati, A.; Garcia-Gonzalo, J.; Seidl, R.; Delzon, S.; Corona, P.; Kolström, M.; et al. Climate change impacts, adaptive capacity, and vulnerability of European forest ecosystems. *For. Ecol. Manag.* **2010**, *259*, 698–709. [CrossRef]
11. Loboda, T.; Krankina, O.; Savin, I.; Kurbanov, E.; Joanne, H. Land Management and the impact of the 2010 extreme drought event on the agricultural and ecological systems of European Russia. In *Land-Cover and Land-Use Changes in Eastern Europe after the Collapse of the Soviet Union in 1991*; Gutman, G., Volker, R., Eds.; Springer International Publishing: Cham, Switzerland, 2017; pp. 173–192.
12. FAO; UNEP. The State of the World's Forests 2020. In *Forests, Biodiversity and People*; FAO: Rome, Italy, 2020; p. 214.
13. Kurbanov, E.; Vorobyev, O.; Leznin, S.; Polevshikova, Y.; Demisheva, E. Assessment of burn severity in Middle Povozhje with Landsat multitemporal data. *Int. J. Wildland Fire* **2017**, *26*, 772–782. [CrossRef]
14. Churchill, D.J.; Jeronimo, S.M.A.; Hessburg, P.F.; Cansler, C.A.; Povak, N.A.; Kane, V.R.; Lutz, J.A.; Larson, A.J. Post-fire landscape evaluations in Eastern Washington, USA: Assessing the work of contemporary wildfires. *For. Ecol. Manag.* **2022**, *504*, 119796. [CrossRef]
15. Souza-Alonso, P.; Saiz, G.; García, R.A.; Pauchard, A.; Ferreira, A.; Merino, A. Post-fire ecological restoration in Latin American forest ecosystems: Insights and lessons from the last two decades. *For. Ecol. Manag.* **2022**, *509*, 120083. [CrossRef]
16. Kukavskaya, E.A.; Buryak, L.V.; Shvetsov, E.G.; Conard, S.G.; Kalenskaya, O.P. The impact of increasing fire frequency on forest transformations in southern Siberia. *For. Ecol. Manag.* **2016**, *382*, 225–235. [CrossRef]
17. Zúñiga-Vásquez, J.M.; Villanueva-Díaz, J.; Cerano-Paredes, J.; Quiñonez-Barraza, G. Impact of fire history on the structure of a temperate forest in Northern Mexico. *Fire* **2023**, *6*, 19. [CrossRef]
18. Fan, Z.; Song, A.; Dong, L.; Alexander, H.D.; Yang, S.; Cheng, N.; Jonathan, L.; Pitchford, J.L. Fire effects on post-invasion spread of Chinese tallow (*Triadica sebifera*) in wet pine flatwood ecosystems in the southeastern United States. *For. Ecol. Manag.* **2021**, *500*, 119658. [CrossRef]
19. Merriam, K.E.; Meyer, M.D.; Coppoletta, M.; Butz, R.J.; Estes, B.L.; Farris, C.A.; North, M.P. Reestablishing natural fire regimes to restore forest structure in California's red fir forests: The importance of regional context. *For. Ecol. Manag.* **2022**, *503*, 119797. [CrossRef]
20. Bergeron, Y.; Gauthier, S.; Flannigan, M.; Kafka, V. Fire regimes at the transition between mixed wood and coniferous boreal forest in Northwestern Quebec. *Ecology* **2004**, *85*, 1916–1932. [CrossRef]
21. Scheper, A.C.; Verweij, P.A.; van Kuijk, M. Post-fire forest restoration in the humid tropics: A synthesis of available strategies and knowledge gaps for effective restoration. *Sci. Total Environ.* **2021**, *771*, 144647. [CrossRef]
22. Rossi, F.S.; de Santos, G.A.A. Fire dynamics in Mato Grosso State, Brazil: The relative roles of gross primary productivity. *Big Earth Data* **2020**, *4*, 23–44. [CrossRef]
23. Hao, B.; Xu, X.; Wu, F.; Tan, L. Long-term effects of fire severity and climatic factors on post-forest-fire vegetation recovery. *Forests* **2022**, *13*, 883. [CrossRef]

24. López-Cruz, S.d.C.; Aryal, D.R.; Velázquez-Sanabria, C.A.; Guevara-Hernández, F.; Venegas-Sandoval, A.; Casanova-Lugo, F.; La O-Arias, M.A.; Venegas-Venegas, J.A.; Reyes-Sosa, M.B.; Pinto-Ruiz, R.; et al. Effect of prescribed burning on tree diversity, biomass stocks and soil organic carbon storage in tropical highland forests. *Forests* **2022**, *13*, 2164. [CrossRef]
25. Bataineh, M.; Portner, B.; Pelkki, M.; Ficklin, R. Prescribed fire first-order effects on oak and maple reproduction in frequently burned upland oak–hickory forests of the Arkansas Ozarks. *Forests* **2022**, *13*, 1865. [CrossRef]
26. Han, Z.; Geng, G.; Yan, Z.; Chen, X. Economic loss assessment and spatial–temporal distribution characteristics of forest fires: Empirical evidence from China. *Forests* **2022**, *13*, 1988. [CrossRef]
27. Kitzberger, T.; Tiribelli, F.; Barberá, I.; Gowda, J.H.; Morales, J.M.; Zalazar, L.; Paritsis, J. Projections of fire probability and ecosystem vulnerability under 21st century climate across a trans-Andean productivity gradient in Patagonia. *Sci. Total Environ.* **2022**, *839*, 156303. [CrossRef] [PubMed]
28. Ponomarev, E.; Zabrodin, A.; Ponomareva, T. Classification of fire damage to boreal forests of Siberia in 2021 based on the dNBR index. *Fire* **2022**, *5*, 19. [CrossRef]
29. Castro, I.; Stan, A.B.; Taiqui, L.; Schiefer, E.; Ghallab, A.; Derak, M.; Fulé, P.Z. Detecting fire-caused forest loss in a Moroccan protected area. *Fire* **2022**, *5*, 51. [CrossRef]
30. Fairman, T.A.; Bennett, L.T.; Nitschke, C.R. Short-interval wildfires increase likelihood of resprouting failure in fire-tolerant trees. *J. Environ. Manag.* **2019**, *231*, 59–65. [CrossRef] [PubMed]
31. Vadrevu, K.P.; Eaturu, A.; Badarinath, K. Fire risk evaluation using multicriteria analysis—A case study. *Environ. Monit. Assess.* **2010**, *166*, 223–239. [CrossRef]
32. Duff, T.J.; Penman, T.D. Determining the likelihood of asset destruction during wildfires: Modelling house destruction with fire simulator outputs and local-scale landscape properties. *Saf. Sci.* **2021**, *139*, 105196. [CrossRef]
33. FAO. *Global Forest Resources Assessment 2020: Main Report*; FAO: Rome, Italy, 2020; p. 184.
34. Barrett, K.; Baxter, R.; Kukavskaya, E.; Balzter, H.; Shvetsov, E.; Buryak, L. Postfire recruitment failure in Scots pine forests of southern Siberia. *Remote Sens. Environ.* **2020**, *237*, 111539. [CrossRef]
35. Smith-Ramírez, C.; Castillo-Mandujano, J.; Becerra, P.; Sandoval, N.; Fuentes, R.; Allende, R.; Acuna, M.P. Combining remote sensing and field data to assess recovery of the Chilean Mediterranean vegetation after fire: Effect of time elapsed and burn severity. *For. Ecol. Manag.* **2022**, *503*, 119800. [CrossRef]
36. Shephard, N.T.; Narine, L.; Peng, Y.; Maggard, A. Climate smart forestry in the southern United States. *Forests* **2022**, *13*, 1460. [CrossRef]
37. Sample, M.; Thode, A.E.; Peterson, C.; Gallagher, M.R.; Flatley, W.; Friggens, M.; Evans, A.; Loehman, R.; Hedwall, S.; Brandt, L.; et al. Adaptation strategies and approaches for managing fire in a changing climate. *Climate* **2022**, *10*, 58. [CrossRef]
38. Kurbanov, E.; Vorobev, O.; Lezhnin, S.; Sha, J.; Wang, J.; Li, X.; Cole, J.; Dergunov, D.; Wang, Y. Remote sensing of forest burnt area, burn severity, and post-fire recovery: A review. *Remote Sens.* **2022**, *14*, 4714. [CrossRef]
39. Somnath, B.; Bikash, R.P.; Gareth, R.; Arvind, C.P.; Prasenjit, A.; Jadunandan, D. Spatio-temporal characterization of landscape fire in relation to anthropogenic activity and climatic variability over the Western Himalaya, India. *GISci. Remote Sens.* **2021**, *58*, 281–299.
40. Qiu, J.; Wang, H.; Shen, W.; Zhang, Y.; Su, H.; Li, M. Quantifying forest fire and post-fire vegetation recovery in the Daxin'anling area of northeastern China using Landsat time-series data and machine learning. *Remote Sens.* **2021**, *13*, 792. [CrossRef]
41. Wang, X.; Di, Z.; Li, M.; Yao, Y. Satellite-derived variation in burned area in China from 2001 to 2018 and its response to climatic factors. *Remote Sens.* **2021**, *13*, 1287. [CrossRef]
42. Koutsias, N.; Karamitsou, A.; Nioti, F.; Coutelieris, F. Assessment of fire regimes and post-fire evolution of burned areas with the dynamic time warping method on time series of satellite images—Setting the methodological framework in the Peloponnese, Greece. *Remote Sens.* **2022**, *14*, 5237. [CrossRef]
43. Alayan, R.; Rotich, B.; Lakner, Z. A Comprehensive framework for forest restoration after forest fires in theory and practice: A systematic review. *Forests* **2022**, *13*, 1354. [CrossRef]
44. Giglio, L.; Loboda, T.; Roy, D.P.; Quayle, B.; Justice, C.O. An active-fire based burned area mapping algorithm for the MODIS sensor. *Remote Sens. Environ.* **2009**, *113*, 408–420. [CrossRef]
45. Xofis, P.; Buckley, P.G.; Takos, I.; Mitchley, J. Long term post-fire vegetation dynamics in north-east Mediterranean ecosystems. The case of mount Athos Greece. *Fire* **2021**, *4*, 92. [CrossRef]
46. dos Santos, S.M.B.; Duverger, S.G.; Bento-Gonçalves, A.; Franca-Rocha, W.; Vieira, A.; Teixeira, G. Remote sensing applications for mapping large wildfires based on machine learning and time series in northwestern Portugal. *Fire* **2023**, *6*, 43. [CrossRef]
47. Morresi, D.; Marzano, R.; Lingua, E.; Motta, R.; Garbarino, M. Mapping burn severity in the western Italian Alps through phenologically coherent reflectance composites derived from Sentinel-2 imagery. *Remote Sens. Environ.* **2022**, *269*, 112800. [CrossRef]
48. Li, X.; Zhang, H.; Yang, G.; Ding, Y.; Zhao, J. Post-fire vegetation succession and surface energy fluxes derived from remote sensing. *Remote Sens.* **2018**, *10*, 1000. [CrossRef]
49. Meneses, B.M. Vegetation recovery patterns in burned areas assessed with Landsat 8 OLI imagery and environmental biophysical data. *Fire* **2021**, *4*, 76. [CrossRef]
50. Maillard, O. Post-fire natural regeneration trends in Bolivia: 2001–2021. *Fire* **2023**, *6*, 18. [CrossRef]

51. Li, X.; Jin, H.; He, R.; Wang, H.; Sun, L.; Luo, D.; Huang, Y.; Li, Y.; Chang, X.; Wang, L.; et al. Impact of wildfire on soil carbon and nitrogen storage and vegetation succession in the Nanweng'he National Natural Wetlands Reserve, Northeast China. *CATENA* **2023**, *221*, 106797. [CrossRef]
52. Bryukhanov, A.V.; Panov, A.V.; Ponomarev, E.I.; Sidenko, N.V. Wildfire impact on the main tree species of the Near-Yenisei Siberia. *Izv. Atmos. Ocean Phys.* **2018**, *54*, 1525–1533. [CrossRef]
53. Kukavskaya, E.A.; Shvetsov, E.G.; Buryak, L.V.; Tretyakov, P.D.; Groisman, P.Y. Increasing fuel loads, fire hazard, and carbon emissions from fires in central Siberia. *Fire* **2023**, *6*, 63. [CrossRef]
54. Bondur, V.G.; Gordo, K.A.; Voronova, O.S.; Zima, A.L.; Feoktistova, N.V. Intense wildfires in Russia over a 22-year period according to satellite data. *Fire* **2023**, *6*, 99. [CrossRef]
55. Kharuk, V.I.; Dvinskaya, M.L.; Ranson, K.J. Fire return intervals within the northern boundary of the larch forest in Central Siberia. *Int. J. Wildl. Fire* **2013**, *22*, 207–211. [CrossRef]
56. Sun, Q.; Burrell, A.; Barrett, K.; Kukavskaya, E.; Buryak, L.; Kaduk, J.; Baxter, R. Climate variability may delay post-fire recovery of boreal forest in southern Siberia, Russia. *Remote Sens.* **2021**, *13*, 2247. [CrossRef]
57. McRae, D.J.; Conard, S.G.; Ivanova, G.A.; Sukhinin, A.I.; Baker, S.P.; Samsonov, Y.N.; Blake, T.W.; Ivanov, V.A.; Ivanov, A.V.; Churkina, T.V.; et al. Variability of fire behavior, fire effects, and emissions in scotch pine forests of central Siberia. *Mitig. Adapt. Strat. Glob. Chang.* **2006**, *11*, 45–74. [CrossRef]
58. Furyaev, V.V. Pyrological regimes and dynamics of the southern taiga forests in Siberia. In *Fire in Ecosystems of Boreal Eurasia. Forestry Sciences*; Goldammer, J.G., Furyaev, V.V., Eds.; Springer: Dordrecht, The Netherlands, 1996; Volume 48.
59. Chu, T.; Guo, X.; Takeda, K. Remote sensing approach to detect post-fire vegetation regrowth in Siberian boreal larch forest. *Ecol. Indic.* **2016**, *62*, 32–46. [CrossRef]
60. Ryzhkova, N.; Pinto, G.; Kryshen', A.; Bergeron, Y.; Ols, C.; Drobyshev, I. Multi-century reconstruction suggests complex interactions of climate and human controls of forest fire activity in a Karelian boreal landscape, North-West Russia. *For. Ecol. Manag.* **2020**, *459*, 117770. [CrossRef]
61. Ostroukhov, A.V. Assessing the extent of landscape fires in the Middle Amur Lowland using long-term satellite data time series. *Curr. Probl. Remote Sens. Earth Space* **2022**, *19*, 164–175.
62. Vorobyov, O.N.; Kurbanov, E.A.; Lezhnin, S.A.; Gubayev, A.V.; Dergunov, D.M.; Tarasova, L.V. Spatio-temporal analysis of forest cover in the Middle Volga using landscape indices and Landsat satellite data. *Curr. Probl. Remote Sens. Earth Space* **2023**, *20*, 144–159. [CrossRef]
63. Perevedentsev, Y.; Sherstyukov, B.; Gusarov, A.; Aukhadeev, T.; Mirsaeva, N. Climate-induced fire hazard in forests in the Volga federal district of European Russia during 1992–2020. *Climate* **2022**, *10*, 110. [CrossRef]
64. Kurbanov, E.A.; Post, W.M. Changes in area and carbon in forests of the Middle Zavolgie: A regional case study of Russian forests. *Clim. Chang.* **2002**, *55*, 157–171. [CrossRef]
65. Kurbanov, E. *Carbon in Pine Forest Ecosystems of Middle Zavolgie, Russia*; Technical Report 2; European Forest Institute: Joensuu, Finland, 2000.
66. Lerink, B.; Hassegawa, M.; Kryshen, A.; Kovalev, A.; Kurbanov, E.; Nabuurs, G.J.; Moshnikov, S.; Verkerk, P.J. Climate-smart forestry in Russia and potential climate change mitigation benefits. In *Russian Forests and Climate Change What Science Can Tell Us 11*; Leskinen, P., Lindner, M., Verkerk, P.J., Nabuurs, G.J., Van Brusselen, J., Kulikova, E., Hassegawa, M., Lerink, B., Eds.; European Forest Institute: Joensuu, Finland, 2020; pp. 73–103.
67. Tamiminia, H.; Salehi, B.; Mahdianpari, M.; Quackenbush, L.; Adeli, S.; Brisco, B. Google Earth Engine for geo-big data applications: A meta-analysis and systematic review. *ISPRS J. Photogramm. Remote Sens.* **2020**, *164*, 152–170. [CrossRef]
68. Gorelick, N.; Hancher, M.; Dixon, M.; Ilyushchenko, S.; Thau, D.; Moore, R. Google Earth Engine: Planetary-scale geospatial analysis for everyone. *Remote Sens. Environ.* **2017**, *202*, 18–27. [CrossRef]
69. Gholamrezaie, H.; Hasanlou, M.; Amani, M.; Mirmazloumi, S.M. Automatic mapping of burned areas using Landsat 8 time-series images in google earth engine: A case study from Iran. *Remote Sens.* **2022**, *14*, 6376. [CrossRef]
70. Roteta, E.; Bastarrika, A.; Ibisate, A.; Chuvieco, E. A preliminary global automatic burned-area algorithm at medium resolution in Google Earth Engine. *Remote Sens.* **2021**, *13*, 4298. [CrossRef]
71. Foga, S.; Scaramuzza, P.L.; Guo, S.; Zhu, Z.; Dilley, R.D.; Beckmann, T.; Schmidt, G.L.; Dwyer, J.L.; Joseph Hughes, M.; Laue, B. Cloud detection algorithm comparison and validation for operational Landsat data products. *Remote Sens. Environ.* **2017**, *194*, 379–390. [CrossRef]
72. Vermote, E.; Justice, C.; Claverie, M.; Franch, B. Preliminary analysis of the performance of the Landsat 8/OLI land surface reflectance product. *Remote Sens. Environ.* **2016**, *185*, 46–56. [CrossRef] [PubMed]
73. Claverie, M.; Vermote, E.F.; Franch, B.; Masek, J.G. Evaluation of the Landsat-5 TM and Landsat-7 ETM+ Surface Reflectance Products. *Remote Sens. Environ.* **2015**, *169*, 390–403. [CrossRef]
74. Roy, D.P.; Kovalskyy, V.; Zhang, H.K.; Vermote, E.F.; Yan, L.; Kumar, S.S.; Egorov, A. Characterization of Landsat-7 to Landsat-8 reflective wavelength and normalized difference vegetation index continuity. *Remote Sens. Environ.* **2016**, *185*, 57–70. [CrossRef]
75. Kennedy, R.E.; Yang, Z.; Gorelick, N.; Braaten, J.; Cavalcante, L.; Cohen, W.B.; Healey, S. Implementation of the LandTrendr Algorithm on Google Earth Engine. *Remote Sens.* **2018**, *10*, 691. [CrossRef]
76. Flood, N. Seasonal composite Landsat TM/ETM+ images using the Medoid (A multi-dimensional median). *Remote Sens.* **2013**, *5*, 6481–6500. [CrossRef]

77. Cohen, W.B.; Yang, Z.; Healey, S.P.; Kennedy, R.E.; Gorelick, N. A LandTrendr multispectral ensemble for forest disturbance detection. *Remote Sens. Environ.* **2018**, *205*, 131–140. [CrossRef]
78. Key, C.H.; Benson, N.C. Landscape assessment: Remote sensing of severity, the normalized burn ratio. In *FIREMON: Fire Effects Monitoring and Inventory System*; USDA Forest Service, Rocky Mountain Research Station, Fort Collins: Denver, CO, USA, 2006; pp. 305–325.
79. Mann, H.B. Nonparametric tests against trend. *Econometrica* **1945**, *13*, 245–259. [CrossRef]
80. Kendall, M.G. *Rank Correlation Methods*; Charles Griffin: Oxford, UK, 1955.
81. Sen, P.K. Estimates of the regression coefficient based on Kendall's tau. *J. Am. Stat. Assoc.* **1968**, *63*, 1379–1389. [CrossRef]
82. Theil, H. A rank-invariant method of linear and polynomial regression analysis. In *Henri Theil's Contributions to Economics and Econometrics*; Springer: Berlin/Heidelberg, Germany, 1992; pp. 345–381.
83. Gocic, M.; Trajkovic, S. Analysis of changes in meteorological variables using Mann-Kendall and Sen's slope estimator statistical tests in Serbia. *Glob. Planet. Chang.* **2013**, *100*, 172–182. [CrossRef]
84. Frazier, R.J.; Coops, N.C.; Wulder, M.A.; Hermosilla, T.; White, J.C. Analyzing spatial and temporal variability in short-term rates of post-fire vegetation return from Landsat time series. *Remote Sens. Environ.* **2018**, *205*, 32–45. [CrossRef]
85. Yuan, J.; Bian, Z.; Yan, Q.; Gu, Z.; Yu, H. An approach to the temporal and spatial characteristics of vegetation in the growing season in Western China. *Remote Sens.* **2020**, *12*, 945. [CrossRef]
86. Hansen, M.C.; Potapov, P.V.; Moore, R.; Hancher, M.; Turubanova, S.A.; Tyukavina, A.; Thau, D.; Stehman, S.V.; Goetz, S.J.; Loveland, T.R.; et al. High-resolution global maps of 21st-century forest cover change. *Science* **2013**, *342*, 850–853. [CrossRef] [PubMed]
87. Congalton, R.G.; Green, K. *Assessing the Accuracy of Remotely Sensed Data: Principles and Practices*, 3rd ed.; CRC Press: Boca Raton, FL, USA, 2019.
88. Xu, Y.; Lin, Z.; Wu, C. Spatiotemporal variation of the burned area and its relationship with climatic factors in Central Kazakhstan. *Remote Sens.* **2021**, *13*, 313. [CrossRef]
89. Canadell, J.G.; Meyer, C.P.; Cook, G.D.; Dowdy, A.; Briggs, P.R.; Knauer, J.; Pepler, A.; Haverd, V. Multi-decadal increase of forest burned area in Australia is linked to climate change. *Nat. Commun.* **2021**, *12*, 6921. [CrossRef] [PubMed]
90. Zhu, Z.; Wulder, M.A.; Roy, D.P.; Woodcock, C.E.; Hansen, M.C.; Radeloff, V.C.; Healey, S.P.; Schaaf, C.; Hostert, P.; Strobl, P.; et al. Benefits of the free and open Landsat data policy. *Remote Sens. Environ.* **2019**, *224*, 382–385. [CrossRef]
91. Vanderhoof, M.K.; Hawbaker, T.J.; Teske, C.; Ku, A.; Noble, J.; Picotte, J. Mapping wetland burned area from Sentinel-2 across the Southeastern United States and its contributions relative to Landsat-8 (2016–2019). *Fire* **2021**, *4*, 52. [CrossRef]
92. Roy, D.P.; Huang, H.; Boschetti, L.; Giglio, L.; Yan, L.; Zhang, H.H.; Li, Z. Landsat-8 and Sentinel-2 burned area mapping—A combined sensor multi-temporal change detection approach. *Remote Sens. Environ.* **2019**, *231*, 111254. [CrossRef]
93. Howe, A.A.; Parks, S.A.; Harvey, B.J.; Saberi, S.J.; Lutz, J.A.; Yocom, L.L. Comparing Sentinel-2 and Landsat 8 for burn severity mapping in Western North America. *Remote Sens.* **2022**, *14*, 5249. [CrossRef]